INTERNATIONAL JOURNAL FOR NUMERICAL METHODS IN FLUIDS
Int. J. Numer. Meth. Fluids 2007; **55**:57–80
Published online 31 January 2007 in Wiley InterScience (www.interscience.wiley.com). DOI: 10.1002/fld.1436

A model of the unsteady response of a backward-facing compliant step

A. G. Gerber*, †, ‡, A. G. L. Holloway and C. Ng

Department of Mechanical Engineering, University of New Brunswick, Fredericton, NB, Canada E3B 5A3

SUMMARY

A large number of industrial surface coating and continuous casting operations require a fluid to flow from a reservoir, over a compliant step, onto a moving substrate. The contact line between the compliant step and substrate in such cases generally responds in an unsteady manner, depending on flow conditions, which can have an important influence on the surface quality of the final product. This work describes the development of a computational fluid dynamics (CFD) model for predicting this unsteady response, with a particular emphasis on isolating the natural frequency of the contact line in a backward-facing step configuration. The compliant step was developed and implemented in the context of a pressure-based finite-element/finite-volume CFD solution, implicit in time, and considers in-surface forces based on a surface tension coefficient or an elastic membrane. Copyright © 2007 John Wiley & Sons, Ltd.

Received 21 October 2005; Revised 7 November 2006; Accepted 12 November 2006

KEY WORDS: compliant step; backward facing; CFD; natural frequency

1. INTRODUCTION

The primary motivation for the present study is the control of surface quality in aluminium continuous (near-net shape) casting operations. The concept of casting a metal to its near final (or net shape) conditions, in terms of dimensions and mechanical properties, has been an intensive area of metal processing research for the past several decades. In casting a metal from its liquid state to its near final conditions leaves little room for correcting surface defects that occur, and therefore increasing attention is being drawn to basic issues behind the delivery of a molten metal to a cooled moving substrate. The complexity involved in the formation of a metal surface at

*Correspondence to: A. G. Gerber, Department of Mechanical Engineering, University of New Brunswick, Fredericton, NB, Canada E3B 5A3.
†E-mail: agerber@unb.ca
‡Associate Professor.

Contract/grant sponsor: NSERC; contract/grant number: CRDPJ-248034

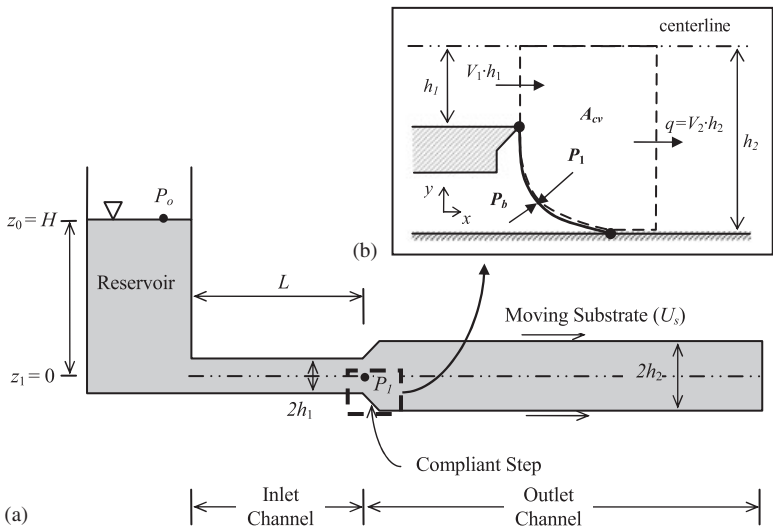

Figure 1. Backward-facing compliant step problem: (a) representative two channel system with intervening compliant step and (b) control volume used in dynamic system model (DSM). Note that the compliant step height is equal to $h = h_2 - h_1$.

the point of liquid/substrate contact is considerable and it is generally required that the problem be simplified for investigation. A first approximation is to describe the problem as a type of backward-facing step flow, but with a compliant step. The compliant step is a moving boundary with the interface having treatments based on the physics of the situation (for example surface tension or membrane). Using this as a basis, the problem has already been addressed from a heat transfer perspective where a fixed compliant step is applied with all of the important heat transfer elements in the vicinity of the liquid/substrate contact [1]. Further to this, the influence of flow and heat transfer on alloy mass transport in this vicinity has also been considered [2]. In these studies the compliant step has been assumed fixed, however, it is well known that the interface responds dynamically to the conditions around it. It is also known that for certain alloys the surface degradation appears as surface markings, or transverse striations, and are a result of contact line movement [3].

This study investigates the backward-facing compliant step movement by developing a methodology to first determine the natural frequency of such a system under isothermal conditions, but developed in a general framework to allow for an increasingly more complex investigation including the presence of heat transfer. Due to the common appearance of the backward-facing geometry and moving substrate in industrial coating operations, it is expected that this model and its results will be of general value to a wide variety of other applications. A simplified schematic of this situation is provided in Figure 1, and provides the basis for describing the subsequent model development and analytical benchmark. The basic features to be highlighted at this point are the location of the compliant step at distance L downstream of a reservoir with hydrostatic head H, moving substrate bounding the outlet channel (top and bottom at distance $2h_2$) downstream of the step, inlet ($2h_1$) channel of length L before the step. The compliant step is shown in Figure 1(b) with details relevant to the dynamic system model (DSM) developed for verification of the results.

DOI: 10.1002/fld

Here, pressures P_b and P_1 are shown outside and inside of the compliant step, respectively, control volume (with area A_{cv} and depth equal to one) adjacent to the compliant step, and the volumetric flow in $(V_1 h_1)$ and out $(V_2 h_2)$ of the control volume.

To allow for many physical features of the compliant step to be investigated, a general model has been developed utilizing finite-element/finite-volume (FE/FV) discretization. Initial research in simulating compliant-boundary motion in the context of a FE/FV computational fluid dynamics (CFD) solution was conducted [4, 5] using an arbitrary-Lagrangian–Eulerian (ALE) approach to handle the mesh motion. The methodology involved a fully coupled solution, where the mesh distribution is solved simultaneously with the compliant-boundary shape and the velocity/pressure variables during time coefficient iterations. The method also yields a distinct interface defining the shape of the compliant boundary; however, the surface cannot fold over on itself as in a breaking wave. Its primary drawback is the complexity of implementation due to the simultaneous coupling of the pressure, velocity, mesh and compliant boundary. It is also difficult to extend to three-dimensional flow situations. The present work draws on this research for the discretization of the interface region, but uses a segregated approach in that the compliant-boundary position is obtained by coefficient loop iteration within a time step. At present no approach is given for incorporating the contact condition at solid/fluid junctures in the solution, and therefore the present work contributes to the extension of the FE/FV method in this area. Furthermore, the authors are not aware of any research that attempts to apply the method to the backward-facing compliant step configuration, with the goal of isolating natural frequency of the contact line. This includes the treatment of the surface as having surface tension or membrane forces, and providing the flexibility of considering oxide layer growth on the compliant boundary. This is a common concern for aluminium which readily forms surface oxides. For future application of the method in-surface force models based on a combination of surface tension and membrane forces is likely.

An important aspect in the simulation of interface movement under the action of surface tension is the contact angle and line where liquids and a solid boundary meet. With interface motion relative to a solid boundary a singularity at the contact line exists, which in the present case is handled with a Navier slip treatment (the details to be discussed subsequently). Associated with the slip treatment is a contact angle that should be determined on the basis of dynamic wetting [6]. Experiments have shown that there is a hysteresis effect around the equilibrium (static) contact angle under dynamic conditions which makes it difficult to determine the contact angle active at the surface. Obtaining a theoretical solution to the dynamic contact angle is currently a very active area of research [7, 8] with no generally applicable model. Considering this uncertainty, for the present work the 'effective' contact angle is chosen to be the static one. This effective contact angle is then applied at all times along the motion of the contact line. Future studies may well investigate this influence by incorporating a model for dynamic contact angle. An example of incorporating a dynamic wetting boundary condition in conjunction with ALE equations and a finite-element fluid flow solver is given in [9].

2. CONSERVATION EQUATIONS

Equations for mass and momentum conservation, applied to the entire domain, are cast in ALE form, which allows for convenient application of mesh motion in the CFD solution. The ALE formulation includes mesh velocities to account for mesh deflection (over a time step) in response to any boundary motions. The relevant conservation equations expressed in Cartesian coordinates

DOI: 10.1002/fld

(x_j) are for mass

$$\frac{\mathrm{d}}{\mathrm{d}t}\int_{V(t)} \rho \,\mathrm{d}V + \int_s \rho(U_j - W_j)\,\mathrm{d}n_j = 0 \tag{1}$$

and momentum

$$\frac{\mathrm{d}}{\mathrm{d}t}\int_{V(t)} \rho U_i \,\mathrm{d}V + \int_s \rho(U_j - W_j)U_i \,\mathrm{d}n_j = -\int_s P \,\mathrm{d}n_i + \int_s \mu\left(\frac{\partial U_i}{\partial x_j} + \frac{\partial U_j}{\partial x_i}\right)\mathrm{d}n_j + \int_s S_{U_i}\,\mathrm{d}V \tag{2}$$

where W_j is the mesh velocity or the velocity of the control-volume boundary surface, and $\mathrm{d}n_j$ (or $\mathrm{d}n_i$) are the differential Cartesian components of the outward normal surface area vector. Other variables are the fluid velocity components, U_j, fluid density, ρ, pressure, P, and dynamic viscosity, μ. Space integration (volume or surface) is over a control volume of volume V and time integration is with $\mathrm{d}t$.

These equations are discretized and solved iteratively for each control volume. During the solution the space conservation law is applied rigorously in the treatment of transient volume terms where

$$\frac{\mathrm{d}}{\mathrm{d}t}\int_V \mathrm{d}V = \int_s W_j \,\mathrm{d}n_j \tag{3}$$

and relates volume changes to the control-volume surface (mesh) velocities.

The modelling of the compliant step begins with balancing the force on the surface, along with a choice of relevant in-surface force model and application of a contact angle (with treatment of the contact line slip) as shown in Figure 2(a). A force balance over a surface area element $\mathrm{d}A_p$, with centre at **P**, along a compliant step involves normal and tangential components resulting from pressure forces, P, in the surface normal direction, traction forces, f, in the tangential direction and in-surface forces. The forces acting at the interface are in equilibrium, which can be expressed

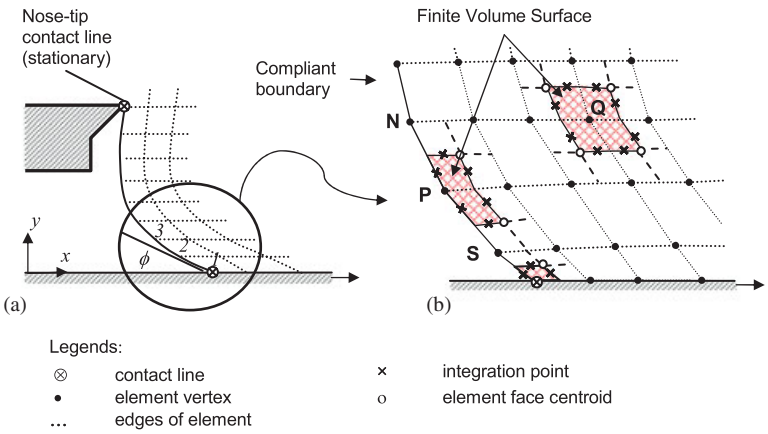

Figure 2. (a) Contact lines and angle for compliant step and (b) FE/FV discretization on a compliant step surface and interior.

DOI: 10.1002/fld

in differential form as

$$(P_1 - P_b)\,\mathrm{d}A_p\mathbf{n}_p + (f_1 - f_b)\mathrm{d}A_p\mathbf{t}_p - \mathbf{T} = 0 \tag{4a}$$

where the in-surface force vector, $\mathbf{T}$, is composed of normal and tangential components

$$\mathbf{T} = \gamma w(\nabla \cdot \mathbf{n})\mathbf{n} + \mathbf{t}(\mathbf{t} \cdot \nabla)\gamma w \tag{4b}$$

where γ is an in-surface tension (units N/m) and w the width of the surface into the 2D plane. From Equation (4), it is clear that the normal component of γw opposes the resultant pressure force, and that the tangential gradient of γw counters the net traction force.

Movement of a compliant step (or boundary) in time requires determining at each new time level the equilibrium position considering any internal surface forces and neighbouring fluid forces governed by Equations (1) and (2). Whenever the boundary is moved, all interior nodes are moved in order to maintain the quality of the grid. The movement of these interior nodes is in accordance with the displacement field D_i, obtained by the solution of the Laplacian equation

$$\frac{\partial}{\partial x_j}\left(\Gamma_\mathrm{m}\frac{\partial D_i}{\partial x_j}\right) = 0 \tag{5}$$

with $D_i = (x_i - x_i^0)$. The mesh stiffness, Γ_m, is a parameter that determines how the nodal displacements are diffused through the domain and can be varied as a function of location or element characteristics.

The boundary conditions for Equations (1) through (3) and (5) are discussed in a subsequent section. The FE/FV discretization and assembly into final coefficient form for solution of velocities and pressure are described in detail in [10]. For closure of the compliant step model (Equation (4)), a model for the in-surface tension is needed, as well as constraints for the two ends conditions on the compliant step. The in-surface tension γ can be modelled in various ways. Its implementation as a model based on the coefficient of surface tension or a flexible elastic membrane will be discussed in the next section. As for the constraints at the two ends of the complaint surface, it is possible to treat them as stationary or as moving contact lines with application of a contact angle as shown in Figure 2(a). In line with the purpose of this paper discretization details are given for the compliant step interface.

3. MODEL OF BACKWARD FACING COMPLIANT STEP

3.1. FE/FV discretization

Figure 2 shows a typical mesh, composed of quadrilateral elements adjacent to a backward-facing compliant step. The element vertices provide the location for finite-volume nodes as shown Figure 2(b). Any internal node **Q** is composed of element quadrants from surrounding elements as illustrated by the crosshatched area in Figure 2(b). This description of a finite volume can also be applied to nodes on the wall or as well along the compliant step at node **P** but with reduced quadrant contributions from surrounding elements. A finite volume forms the basis for discrete conservation equations obtained by integrating over a control volume with surface fluxes evaluated using conditions located at integration points as shown in Figure 2(b). This describes in principle the mesh structure behind the FE/FV discretization process. However, obtaining a solution for the

DOI: 10.1002/fld

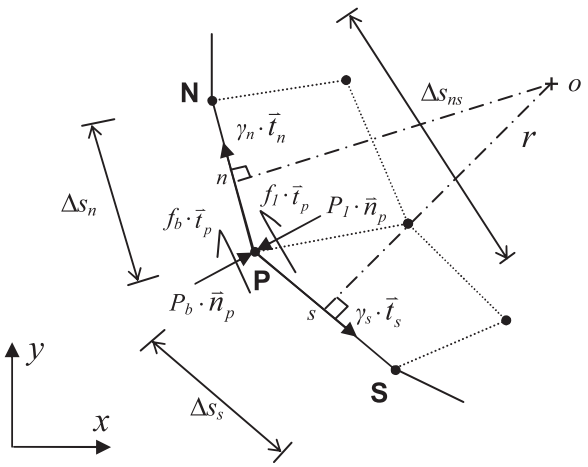

Figure 3. Surface stresses and in-surface tensions used in force balance on compliant discrete interface. An arc of radius r (not shown) passes through nodes **N**, **P** and **S** defining segment **n**–**P**–**s** of the compliant step.

control-volume values must be obtained in conjunction with a model for the surface forces in the compliant step and its motion.

3.2. Compliant step

3.2.1. Surface forces. The corresponding surface stresses and in-surface tensions are shown in Figure 3. The force balance when applied to node **P**, over a discrete area A_p, and using piecewise-linear segments, Equation (4a) results in a vector equation of the form

$$(P_1 - P_b)A_p\mathbf{n}_p + (f_1 - f_b)A_p\mathbf{t}_p - T_s\mathbf{t}_s + T_n\mathbf{t}_n = 0 \tag{6}$$

The normal pressures, traction stresses and in-surface forces are all directed according to unit vectors calculated on the following basis:

$$\mathbf{n}_p = \left(-\frac{y_N - y_S}{\Delta s_{ns}}\,\mathbf{i},\ \frac{x_N - x_S}{\Delta s_{ns}}\,\mathbf{j}\right) \quad \text{normal to node } \mathbf{P};\ \text{pointing outward from the fluid } (P_1 \text{ to } P_b)$$

$$\mathbf{t}_p = \left(\frac{x_N - x_S}{\Delta s_{ns}}\,\mathbf{i},\ \frac{y_N - y_S}{\Delta s_{ns}}\,\mathbf{j}\right) \quad \text{tangent to node } \mathbf{P};\ \text{pointing from } \mathbf{S} \text{ to } \mathbf{N}$$

$$\mathbf{t}_s = \left(\frac{x_P - x_S}{\Delta s_s}\,\mathbf{i},\ \frac{y_P - y_S}{\Delta s_s}\,\mathbf{j}\right) \quad \text{tangent to surface segment } \mathbf{P}\text{–}\mathbf{S};\ \text{pointing from } \mathbf{S} \text{ to } \mathbf{P}$$

$$\mathbf{t}_n = \left(\frac{x_N - x_P}{\Delta s_n}\,\mathbf{i},\ \frac{y_N - y_P}{\Delta s_n}\,\mathbf{j}\right) \quad \text{tangent to surface segment } \mathbf{P}\text{–}\mathbf{N};\ \text{pointing from } \mathbf{P} \text{ to } \mathbf{N}$$

where references to upper case **S**, **P** and **N** and lower case s, n indicate locations as shown in Figure 3. The coordinates x, y are located on the basis of their subscripts at locations depicted in

DOI: 10.1002/fld

Figure 3. Additional geometric quantities are A_p defined as

$$A_p = \frac{(\Delta s_s + \Delta s_n)}{2} w$$

and the linear distances as

$$\Delta s_n = \sqrt{(x_N - x_P)^2 + (y_N - y_P)^2}$$

$$\Delta s_s = \sqrt{(x_P - x_S)^2 + (y_P - y_S)^2}$$

$$\Delta s_{ns} = \sqrt{(x_N - x_S)^2 + (y_N - y_S)^2}$$

Equation (6) is assembled for all the nodes along the compliant step. Pressure and traction information is obtained from the flow solution by solving at the control-volume locations in Figure 2. In order to solve for the x, y locations of the compliant step nodes, models are needed for the in-surface forces which are described next.

3.2.2. In-surface forces. The compliant step can be modelled with in-surface forces determined on the basis of a coefficient of surface tension or as a flexible elastic membrane. In our present study, when the in-surface force, γw, in Equation (4) is represented with a coefficient of surface tension, along with an assumption of isothermal flow, the tangential component of $\mathbf{T}$ in Equation (4b) becomes zero. Correspondingly the traction forces must be zero, and the remaining applied pressure forces are in equilibrium with the normal in-surface force component. However when the compliant step is modelled as elastic, where γw changes depending on the degree of localized 'stretching' of the interface, tangential in-surface force variations are also present along with surface traction forces. The state of $\mathbf{T}$ should be kept in mind when considering the two models that follow.

For an isothermal flow the in-surface tension, γ, can be equated to the coefficient of surface tension, σ, so that

$$\gamma = \sigma \tag{7a}$$

A surface modelled with Equation (7a) will also be referred to as a meniscus in this paper. An alternative model for γ is to treat the surface as a flexible elastic membrane. This membrane resists deflection from an equilibrium (un-stressed) length, Δs_0, and has a membrane (or spring) constant, which is analogous to Young's modulus, shown here as K. The in-surface force is then

$$\gamma = K(\Delta s - \Delta s_0) \tag{7b}$$

where Δs is the new segment length calculated as a function of the nodal positions on the surface. A surface modelled with Equation (7b) will be referred to as a membrane.

3.2.3. Contact line model. Two geometric constraints are required for the compliant step, and in the case of a liquid/air surface tension controlled interface are to be given as contact lines as indicated in Figure 2(a). The nose-tip contact line is assumed to be stationary and at the leading edge of the compliant step as shown. For this condition to be stable requires the cut-back angle (angle α as described in Appendix A) to be greater than the static contact angle for all positions of the meniscus. The substrate contact line, however can have motion, at a specified contact angle,

DOI: 10.1002/fld

along the substrate but not normal to it. This motion is possible because of a Navier slip treatment of the singularity located there.

The singularity at the contact line leads to an infinite force tangential to the solid boundary which must be relieved by applying a slip model. A common approach is the Navier slip condition [11]. In this treatment a model is applied to relate the slip proportionally to the fluid stress at the wall. In the present model this is achieved implicitly by solving control volumes (for mass and momentum) centred at the contact line as shown in Figure 2(b). Assembly of the discrete control-volume momentum equation incorporates the wall fluid shear stress, along with contributions from neighbouring nodes. The iterative solution of the equations (described more completely in the next section), which includes forces applied in and along the compliant step, yields a volume averaged velocity and pressure located at the contact line node. The contact line velocity (which is also obtained as part of the iterative solution) and substrate speed (which is a fixed boundary condition) bound this nodal velocity. The contact line velocity, including its position, are therefore obtained proportional to the fluid wall shear stress, with the proportionality determined on the basis of conservation principles around the contact line.

It should be mentioned here that the treatment of the slip condition is open to various options, and some studies recently have indicated that the form of the model does not have much influence on the shape of the interface away from the singularity [8, 12]. In the present case grid refinement studies indicated no troubles in convergence as the mesh sizing, approaching the singularity, was decreased.

While applying a Navier slip treatment at the contact line node, an 'effective' contact angle is maintained equal to a non-wetting static contact angle, ϕ, as illustrated in Figure 2(a). Two assumptions are made for applying the static contact angle, namely; (a) the substrate contact line is to stay in contact with the surface and therefore y_1 in Figure 2(a) is constant and known; and (b) the static contact angle ϕ is specified and preserved at all times (no variation of dynamic contact angle). Therefore, for the constraint at the substrate, the term including γ_s, representing the influence of the in-surface force from the boundary node (i.e. substrate contact line), in Equation (6) is replaced with

$$\gamma_s w \cdot \mathbf{t}_s = \sigma\, w \cdot \left(-\cos\phi\, \frac{x_P - x_S}{\Delta S_s} + \sin\phi\, \frac{y_P - y_S}{\Delta S_s} \right) \tag{8}$$

Note that for this boundary node, node **P** and **S** are node 2 and 1, respectively. The negative sign in the cosine term accounts for the directional effect and w is taken as 1.

The position of the node adjacent to the substrate contact line (x_2, y_2), along with the static contact angle ϕ, gives the relation (see Figure 2(a)):

$$\tan\phi = -\frac{y_2 - y_1}{x_2 - x_1} \tag{9}$$

where (x_1 , y_1) is the position of the substrate contact line with y_1 known (assumption (a) previously stated) and x_1 unknown. With the solution for (x_2, y_2) (obtained by solving Equation (6) in a manner as described in the next section) then x_1 can be back calculated and gives the contact position, x_c, reported in subsequent results.

DOI: 10.1002/fld

4. SOLUTION METHODOLOGY

4.1. Solution of compliant step equations

The previous section describes the discretization of the compliant step including boundary conditions. From this a coupled set of force balance equations (in x and y) can be assembled at each node. The nodal equations are obtained by expanding the unit vectors in Equation (6) and considering only the compliant step motion in the x and y directions, we arrive at

$$\sum F_x = 0$$

$$-ay_N + ay_S + (b+d)x_N - (b+c)x_S + (c-d)x_P = 0 \tag{10}$$

$$\sum F_y = 0$$

$$ax_N - ax_S + (b+d)y_N - (b+c)y_S + (c-d)y_P = 0 \tag{11}$$

with coefficients (where $w = 1$) defined as

$$a = +\left[(P_1 - P_b) \cdot \frac{\Delta s_s + \Delta s_n}{2 \cdot \Delta s_{NS}}\right]$$

$$b = \left[(f_1 - f_b) \cdot \frac{\Delta s_s + \Delta s_n}{2 \cdot \Delta s_{NS}}\right]$$

$$c = -\frac{\gamma_s}{\Delta s_s}$$

$$d = \frac{\gamma_n}{\Delta s_n}$$

The force balance equations assembled for each node can be written in correction form by substituting

$$\begin{aligned} x_Q &= x_Q^0 + x'_Q \\ y_Q &= y_Q^0 + y'_Q \end{aligned} \tag{12}$$

into Equations (10) and (11), respectively, and collecting the terms, where $Q = N$, S or P. Note that in Equation (12) x_Q^0 and y_Q^0 represents the latest known interface positions, while x'_Q and y'_Q become the unknowns and are the corrections required to obtain the exact solution. The resulting matrix represents a coupled system since each nodal force equation depends on the solution of x' and y'. We then have

$$[A]\{X'\} = \{B\} \tag{13}$$

where A is the matrix of all related coefficients, X' is the vector solution for correction values $\{x'_1, y'_1, x'_2, y'_2, \ldots, x'_n, y'_n\}$ and B is the vector of known variables and boundary condition information.

DOI: 10.1002/fld

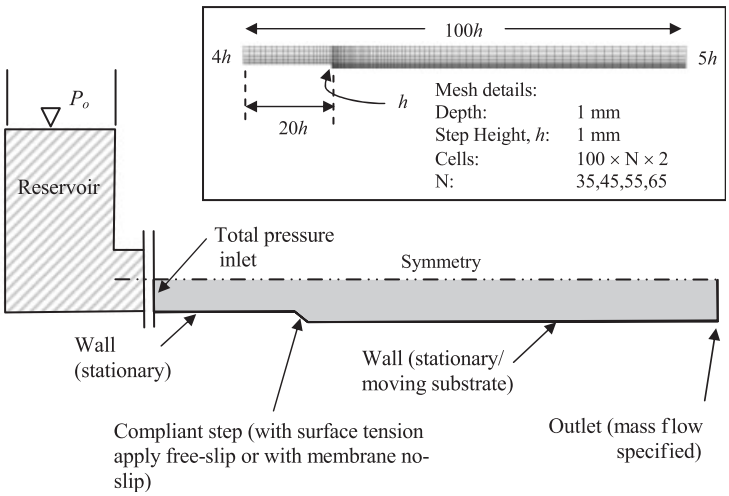

Figure 4. Dimensions and boundary treatments for the backward-facing compliant step model. Note for the CFD solution the reservoir influence is embedded in the total pressure inlet condition, assuming no upstream losses and that the reservoir is far removed (allowing a symmetry condition to be employed).

The resulting system of equations is highly non-linear. In the present case a direct matrix solution is used with iterative refinement, by repeated application of Equation (12), which when converged (the sum of vector X' is driven to a small number) gives the new boundary position. The new x and y boundary coordinates are obtained at node locations which are a function of pressure and velocity when two-way coupling is active.

4.2. Coupled CFD and compliant step solution

4.2.1. Model geometry and boundary conditions. The geometry of the CFD model is shown in Figure 4, *via* the shaded zone, and resembles the geometry of a typical backward-facing step except for the inclusion of the compliant step as indicated. All dimensions shown are scaled in terms of the height of the compliant boundary, here given with dimension h $(=h_2 - h_1)$. For these tests a structured grid is used, although not required for the CFD solver, with noticeable refinement near the wall and across the compliant surface as seen in the upper right corner of Figure 4 (in this inset N refers to the number of nodes applied along the compliant step).

A total pressure and mass flow specified boundary conditions are applied to inlet and outlet, respectively. A stationary no-slip wall condition is applied along the inlet channel (refer also to Figure 1(a)) while the substrate, along the exit channel, uses a no-slip condition with a wall moving at a specified speed. Along the compliant step a free-slip wall is applied with a surface tension coefficient in-surface model (since isothermal conditions prevail) or a no-slip wall with a membrane. The position of the compliant step along this boundary is calculated based on the models previously described. The remaining surfaces are defined as planes of symmetry.

4.2.2. CFD solution methodology. The compliant step model is implemented such that the shape of the meniscus is solved at the beginning of each coefficient loop within a transient CFD solution. A number of coefficient loops are solved within a time step to resolve all non-linearities in the

DOI: 10.1002/fld

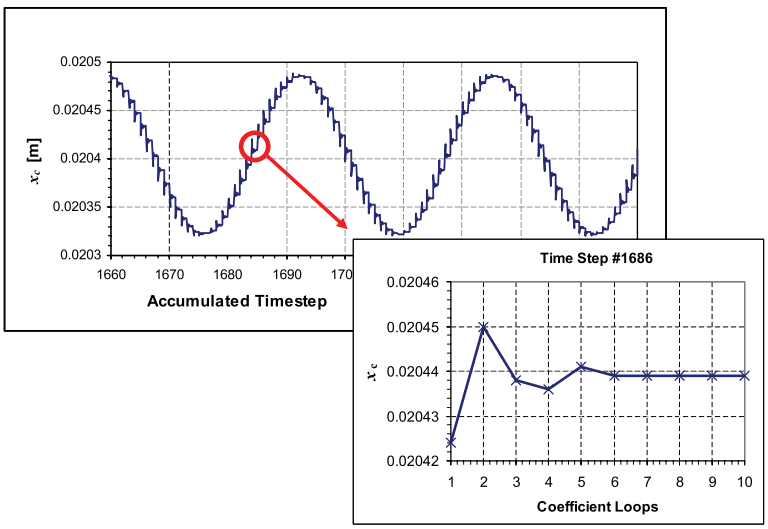

Figure 5. Typical response of the contact line location, x_c, in transient simulation with oscillating hydrostatic head H. Inset shows contact line convergence behaviour within time-step coefficient loop iterations.

coefficients for both the fluid flow equations and the compliant step. The compliant step model solves the force balance equations (Equations (10) through (13)) using surface pressures (and traction stresses for a membrane) available at the end of the previous coefficient loop and returns the x, y positions defining the new boundary. The boundary of the mesh is moved accordingly, with this movement diffused into the remaining mesh by solving a mesh displacement equation (Equation (5)). The new mesh coordinates and associated mesh velocities, W_j, are used for the subsequent solution of the momentum (U_j) and mass (P) equations. The resulting effect is a very strong coupling between the flow field and the compliant step. Several coefficient loop iterations are usually required within a time step to resolve this non-linearity. This iteration process is highlighted in Figure 5 by monitoring the location of the contact line, x_c, after each coefficient loop solution for a flow with oscillating total pressure inlet conditions. As can be seen in the inset, convergence within a time step of the contact line location was generally achieved within 10 coefficient loops or less.

The compliant step solution was implemented into a general purpose commercial CFD solver ANSYS-CFX, which is based on a FE/FV discretization of the conservation equations as described earlier. While spatial discretization is second-order accurate, the transient uses a first-order backward Euler scheme in this work. The solution of the fluid flow system of equations is accelerated through the use of a linear multigrid solver [13] and a coupled solution of the momentum and mass equations [14]. Specific details on the convergence criteria for the compliant step model, the mesh motion and conservation equations (for the CFD model) are as follows:

(a) *Force balance equation* (*Equation* (6)): The sum of the corrections X' after each direct solution of Equation (13) is normalized against the height of the nose-tip, h. These normalized residuals are required to be reduced to below 1×10^{-5} during the iterative solution.

DOI: 10.1002/fld

(b) *Mesh motion*: As the boundary is moved the mesh motion equation (Equation (5)) is solved to ensure high quality elements are maintained in the vicinity of the compliant step. An RMS residual convergence criteria for this equation is set at 1×10^{-7}. The tight convergence ensures that all boundary motions have been sufficiently diffused into the interior mesh.
(c) *Conservation equations*: The conservation equations for mass and momentum (Equations (1) and (2)), when coupled with the compliant step model, are solved to RMS residuals below 1×10^{-4} during coefficient loop iterations within each time step.

5. VERIFICATION OF CFD MODEL

5.1. Analytical benchmarks—dynamic system model (DSM)

The present problem can be represented as a simplified fluid system composed of a reservoir and two flow channels with an intervening compliant step, as illustrated in Figure 1 and described in the Introduction. The reservoir is open to atmosphere and has a liquid-level at $z_0 = H$. It is desired to determine the natural frequency response of the compliant step when treated as an air/liquid interface with a constant coefficient of surface tension (isothermal conditions), and stimulated by variation in the liquid level H. We first accomplish this by developing a DSM for the problem assuming one-dimensional flow, and afterwards compare the results to solutions obtained by the CFD model for this simplified case.

The oscillating behaviour of the compliant step may be described by the unsteady form of Bernoulli's equation applied along a streamline (from point 0 to 1) in the form

$$\frac{P_0}{\rho g} + \frac{U_0^2}{2} + z_0 = \frac{P_1}{\rho g} + \frac{U_1^2}{2g} + z_1 + \frac{L}{g}\frac{\mathrm{d}U_1}{\mathrm{d}t} + K\frac{U_1^2}{2g} \tag{14}$$

where near the compliant step P_1 is the average local pressure and U_1 is the average velocity with both varying in time. In addition P_0 is the fixed atmospheric pressure above the reservoir, and K is a friction factor accounting for losses along the flow path. The hydostatic head H $(= z_0 - z_1)$, is allowed to change with time and g is the gravitational constant.

Dividing Equation (14) through by L/g and taking the time derivative of each term results in a second-order differential equation describing the fundamentals of a dynamic system

$$\frac{\mathrm{d}^2U_1}{\mathrm{d}t^2} = \frac{g}{L}\frac{\mathrm{d}H}{\mathrm{d}t} - \frac{1}{\rho L}\frac{\mathrm{d}P_1}{\mathrm{d}t} - \frac{(K+1)}{L}V_1 \cdot \frac{\mathrm{d}U_1}{\mathrm{d}t} \tag{15}$$

In order to relate the velocity and pressure, and render the equation solvable, we look at a control volume that encompasses a region just past the nose-tip, as shown in Figure 1(b). This control volume encompasses a region of fluid at half the height of the flow channel and, most importantly, adjoining the compliant step. The control volume will deform as the shape of the meniscus changes. Within this control volume, it is assumed that the pressure remains spatially uniform but varies with time.

For a deformable control volume with incompressible flow, the conservation of mass can be written, in terms of volumetric flow rate per unit depth, as

$$\frac{\mathrm{d}}{\mathrm{d}t}(A_{\mathrm{cv}}) = U_1 h_1 - q \tag{16}$$

DOI: 10.1002/fld

where A_{cv} is the area of the control volume, $U_1 h_1$ and q are the instantaneous flow rates entering and leaving the control volume, respectively. Furthermore, q is the desired output flow rate in a controlled coating process and is assumed to be constant.

Next, assuming the compliant step is treated as a meniscus the pressure across the interface is defined as

$$P_1 - P_b = \sigma\kappa \tag{17}$$

where P_b is the pressure of the air gap behind the meniscus and is assumed to be constant. In addition κ is the curvature of the meniscus equal to r^{-1}. Applying the chain rule, we can relate the time variation of pressure, $\mathrm{d}P_1/\mathrm{d}t$, to the mass balance for the control volume (Equation (16)) and the curvature of the meniscus (by taking derivative of Equation (17), with respect to κ), so that

$$\frac{\mathrm{d}P_1}{\mathrm{d}t} = \frac{\mathrm{d}P_1}{\mathrm{d}\kappa} \cdot \frac{\mathrm{d}\kappa}{\mathrm{d}A_{cv}} \cdot \frac{\mathrm{d}A_{cv}}{\mathrm{d}t}$$

where the resulting equation after substitution is

$$\frac{\mathrm{d}P_1}{\mathrm{d}t} = \frac{\mathrm{d}\kappa}{\mathrm{d}A_{cv}} \cdot (U_1 h_1 - q) \cdot \sigma \tag{18}$$

and where $\mathrm{d}\kappa/\mathrm{d}A_{cv}$ is the curvature *versus* area relationship of the meniscus and is a function of the geometry and contact angle.

By substituting Equation (18) into Equation (15) one obtains

$$\frac{\mathrm{d}^2 U_1}{\mathrm{d}t^2} + \frac{(K+1)}{L} U_1 \cdot \frac{\mathrm{d}U_1}{\mathrm{d}t} + \frac{h_1 \sigma}{\rho L} \cdot \frac{\mathrm{d}\kappa}{\mathrm{d}A_{cv}} \cdot U_1 = \frac{g}{L} \frac{\mathrm{d}H}{\mathrm{d}t} + \frac{q\sigma}{\rho L} \cdot \frac{\mathrm{d}\kappa}{\mathrm{d}A_{cv}} \tag{19}$$

Using prime notation and coefficients, Equation (19) is rewritten and expressed as

$$y'' + C_1 y \cdot y' + C_2 y = f(t)$$

The resulting differential equation represents a second-order system with non-linear damping coefficient of $C_1 y$, a spring constant of C_2 and a forcing function of $f(t)$. This non-linear system is of single degree-of-freedom since solving y and its time derivatives will reveal sufficient information to understand the basic characteristics of the system.

5.2. Meniscus frequency and damping

Rather than solving this non-linear differential equation, Equation (19) will be linearized by rewriting the dependent variables in terms of its equilibrium values plus a deviation. Hence, Equation (19) becomes

$$\frac{\mathrm{d}^2 \delta U_1}{\mathrm{d}t^2} + \frac{(K+1)}{L}(U_{1\mathrm{eq}} + \delta U_1) \cdot \frac{\mathrm{d}\delta U_1}{\mathrm{d}t} + \frac{h_1 \sigma}{\rho L} \cdot \frac{\mathrm{d}\kappa}{\mathrm{d}A} \cdot (U_{1\mathrm{eq}} + \delta U_1) = \frac{g}{L} \frac{\mathrm{d}\delta H}{\mathrm{d}t} + \frac{q\sigma}{\rho L} \cdot \frac{\mathrm{d}\kappa}{\mathrm{d}A} \tag{20}$$

For the equilibrium conditions, $\mathrm{d}U_1/\mathrm{d}t = 0$, $\mathrm{d}H/\mathrm{d}t = 0$ and Equation (16) reduces to

$$U_{1\mathrm{eq}} = \frac{q}{h_1} \tag{21}$$

DOI: 10.1002/fld

The resulting equilibrium average velocity can be substituted into the unsteady Bernoulli's equation (Equation (14)) yielding an equilibrium pressure P_{1eq}, which then is substituted into Equation (17) to get the curvature κ_{eq}, so that finally

$$P_{1eq} - P_0 = \rho g H_{eq} - (K+1)\frac{\rho U_{1eq}^2}{2} \tag{22}$$

$$\kappa_{eq} = \frac{1}{\sigma}\left[\rho g H_{eq} - (K+1)\frac{\rho U_{1eq}^2}{2} + P_0 - P_b\right] \tag{23}$$

These equilibrium values can be applied to the geometry constructed in Figure 1(b) in evaluating the equilibrium area and, subsequently, giving the static stiffness $d\kappa/dA$, of the fluid system near equilibrium conditions, i.e. $(d\kappa/dA)_{eq.}$ Details on how $d\kappa/dA$ is calculated is given in Appendix A.

All the equilibrium values (U_{1eq}, P_{1eq} and $(d\kappa/dA)_{eq}$) derived thus far are used in the linearization. Under a small amplitude oscillation assumption, $\delta U_1\, d\delta U_1$ is assumed to be much smaller than δU_1 (in Equation (20)) and is negligible. The resulting linearized equation is

$$\frac{d^2\delta U_1}{dt^2} + \frac{(K+1)}{L}\left(\frac{q}{h_1}\right)\cdot\frac{d\delta U_1}{dt} + \left(\frac{h_1\sigma}{\rho L}\cdot\left.\frac{d\kappa}{dA}\right|_{eq}\right)\cdot\delta U_1 = \frac{g}{L}\frac{d\delta H}{dt} \tag{24}$$

or in terms of prime notation and coefficients as

$$y'' + C_1\left(\frac{q}{h_1}\right)\cdot y' + C_2 y = f(t)$$

Such a linearized system would have an undamped natural frequency of

$$f_n = \frac{1}{2\pi}\sqrt{C_2} = \frac{1}{2\pi}\sqrt{\frac{h_1\sigma}{\rho L}\cdot\left.\frac{d\kappa}{dA}\right|_{eq}} \tag{25}$$

And a damping ratio of

$$\zeta = \frac{C_1(q/h_1)}{2\sqrt{C_2}} = \frac{q(K_{eq}+1)}{2h_1 L\sqrt{\dfrac{h_1\sigma}{\rho L}\cdot\left.\dfrac{d\kappa}{dA}\right|_{eq}}} \tag{26}$$

These two parameters are important in characterizing a dynamic system. More emphasis will be given to the undamped natural frequency when verifying the CFD model in the subsequent section. The one-dimensional analysis provides no information on the friction factor K_{eq} which for the purpose of the present work is not required. It is clear that a key parameter in evaluating the frequency and damping parameters is the curvature to area derivative present in both Equations (25) and (26). An accurate determination of this is given in Appendix A.

6. RESULTS AND DISCUSSION

A common method used by engineers to determine the characteristics of a system is the step input test. The response of a step input can be used to determine the undamped natural frequency and

DOI: 10.1002/fld

Table I. Parameters used in CFD simulations in comparison with DSM predictions.

Parameter	Symbol	Unit	Water	Aluminium
Fluid parameters				
Density	ρ	kg/m^3	997	2370
Coefficient of surface tension	σ	N/m	71.7×10^{-3}	850×10^{-3}
Dynamic viscosity	μ	N s	8.899×10^{-4}	2.37×10^{-3}
Contact angle	θ	deg.	140	140
Geometric parameters				
Upstream channel	h_1	m	0.004	0.004
Downstream channel	h_2	m	0.005	0.005
Step height	h	m	0.001	0.001
Channel length (upstream)	L	m	0.02	0.02
Process parameters				
Head	H	mm	7.5	37.3
Flow rate per unit width	q	m^2/s	0.48×10^{-3}	1.05×10^{-3}
Substrate speed	U_s	m/s	0.1	0.1
Dimensionless parameters				
Head	$\eta = \rho g h H/\sigma$		1.02	1.02
Reynold number	$Re = \rho q/\mu$		536	1055
Weber number	$We = h\sigma/q^2\rho$		3.2×10^{-1}	3.1×10^{-1}
Frequency	$\Phi = f_n \rho^{1/2} h^{3/2}/\sigma^{1/2}$		8.81	8.82

Note: Properties for water taken at 300 K and those for aluminium at a temperature that matches kinematic viscosity ($=\mu/\rho$) between water and aluminium.

damping ratio of a system. As a test to the CFD model a step input is applied by increasing the total pressure at the inlet boundary (equivalent to a step increase in the reservoir head) from a previously converged solution using a rigid compliant step. The transient motion of the meniscus is captured by observing the location of the substrate contact line, x_c. For these compliant step simulations, conducted for water and aluminium, the geometric and fluid parameters are given in Table I.

The geometric and fluid parameters were chosen in order to meet certain similarity constraints between the water and aluminium system. Based on a previous study of an experimental water model of the backward-facing compliant step configuration [15], dimensional analysis suggests that the key dimensionless parameters for a horizontal arrangement are $\Phi = f(Re, We, \eta, \phi)$, with each parameter defined in Table I. Initial water studies suggested that the *Re* dependence is small, and this is tested in the present case by simulating conditions at different Reynolds numbers and monitoring Φ. As shown in Table I, for two different Reynolds numbers Φ remains nearly the same when We, η, ϕ remain fixed, supporting the initial observation of a weak Reynolds number dependence. Using the same fluid parameters the model was then subsequently compared to the DSM model results with an emphasis on natural frequency predictions, given in terms of a dimensionless frequency Φ, and its dependence on η.

Comparison to the DSM model begins with Figure 6 showing the response of x_c for a water and aluminium meniscus both with a contact angle of 140° (it is assumed that a surface treatment to the substrate can be applied for water to give a contact angle similar to aluminium). Both results

DOI: 10.1002/fld

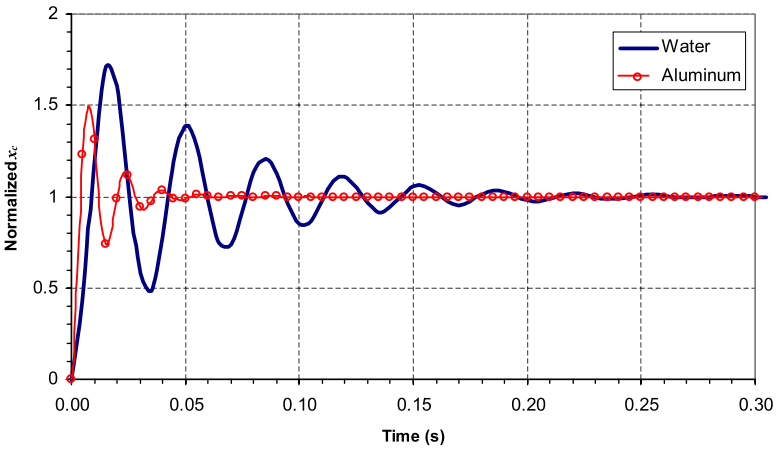

Figure 6. Contact line response with step input applied to water and aluminium meniscus (conditions as given in Table I). Contact line location normalized by the final equilibrium position $x_c/h = 0.376$ obtained after step input.

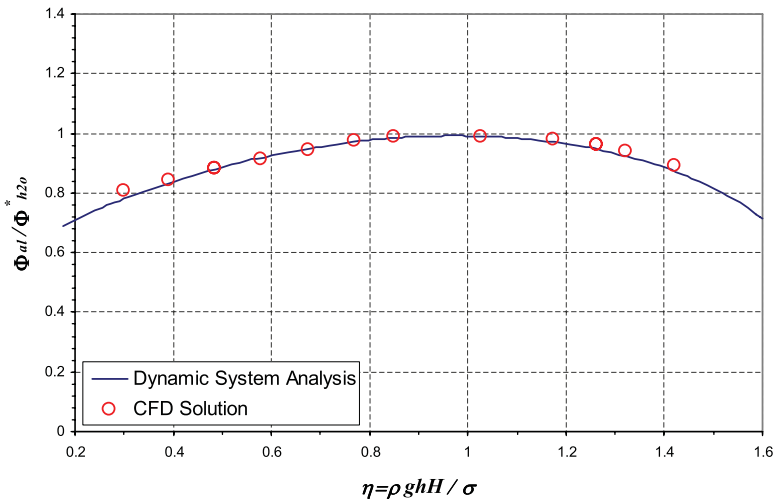

Figure 7. Comparison of predictions of dimensionless oscillation frequency between CFD and DSM with both results normalized by the oscillation frequency of water obtained at $\eta = 1.02$. Conditions for the simulations are as outlined in Table I with $We = 3.1 \times 10^{-1}$ and $\phi = 140°$ (results independent of Re).

can be identified as a typical response of a second-order system. The rapid decay observed in the aluminium contact location is a result of a higher damping ratio when compared to the water meniscus. Postprocessing yields an undamped natural frequency (f_n) of 29.7 Hz for water and 66.2 Hz for aluminium, and damping ratios 0.09 for water and 0.21 for aluminium. Only natural frequency can be compared to the analytical DSM result given by Equation (25), which gives the corresponding values of 31.9 and 71.2 Hz. The results of this comparison are very promising, in

DOI: 10.1002/fld

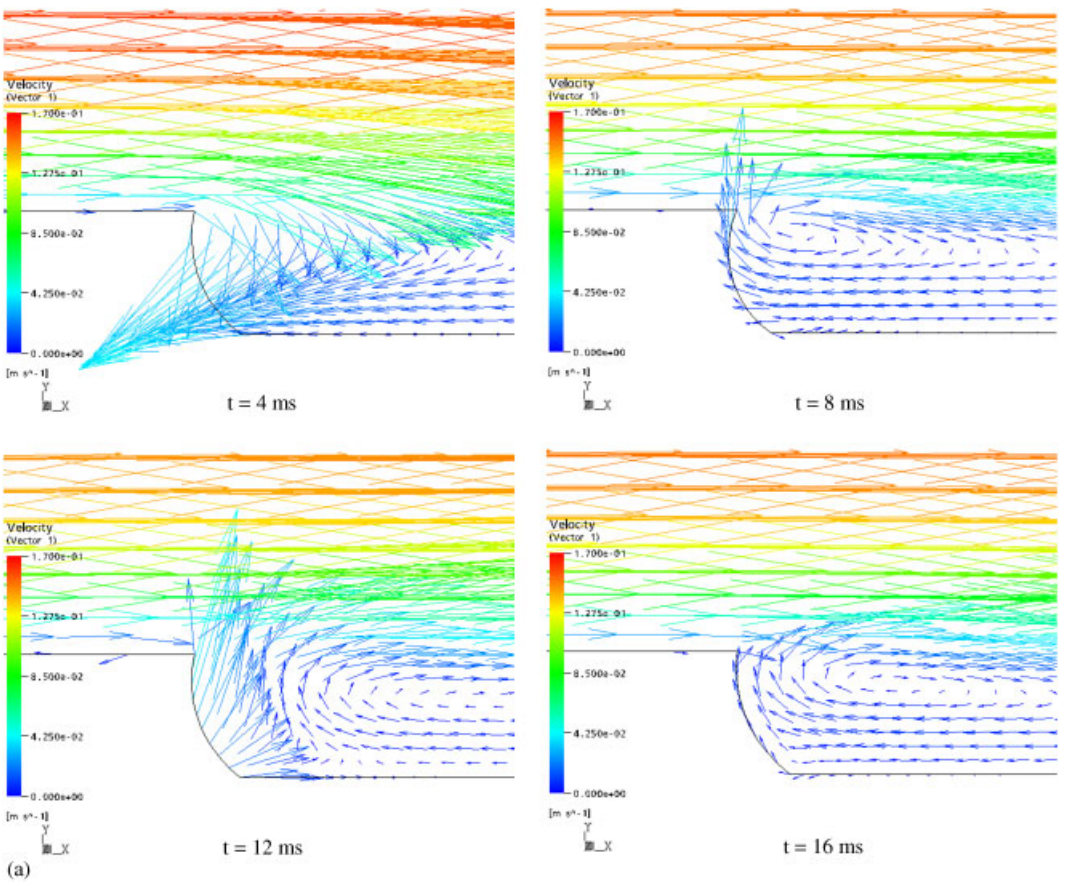

Figure 8. Meniscus compliant step response, with local velocity field, following step input for: (a) stationary substrate; and (b) moving substrate at a speed of 0.1 m/s. Results obtained with conditions as outlined in Table I.

particular comparing the CFD predicted ratio of water to aluminium natural frequencies to that obtained by the analytical benchmark give the same value of 2.23.

The above step input test was expanded to include a range of CFD simulations with different non-dimensional head η (definition given in Table I) ranging from 0.3 to 1.4. The predicted dimensionless (natural) frequency Φ_{al} was normalized against the peak water value Φ^*_{h2o} also obtained by CFD, and compared in Figure 7 to the benchmark DSM results using Equation (25). This comparison is again very good, with the CFD and DSM predictions showing the same peak dimensionless natural frequency very close to $\eta = 1$.

Since Equation (25) suggests a natural frequency that is not dependent on substrate speed U_s, this was tested in the CFD model by varying the substrate speed while maintaining conditions given in Table I. Solutions were thus obtained at speeds 0.0, 0.1, 0.5, 1.0 and 1.5 m/s, and all indicated only a minor influence (differences less than 2% relative to 66.2 Hz obtained with conditions in Table I) on the predicted natural frequency lending support to the form of Equation (25). While

DOI: 10.1002/fld

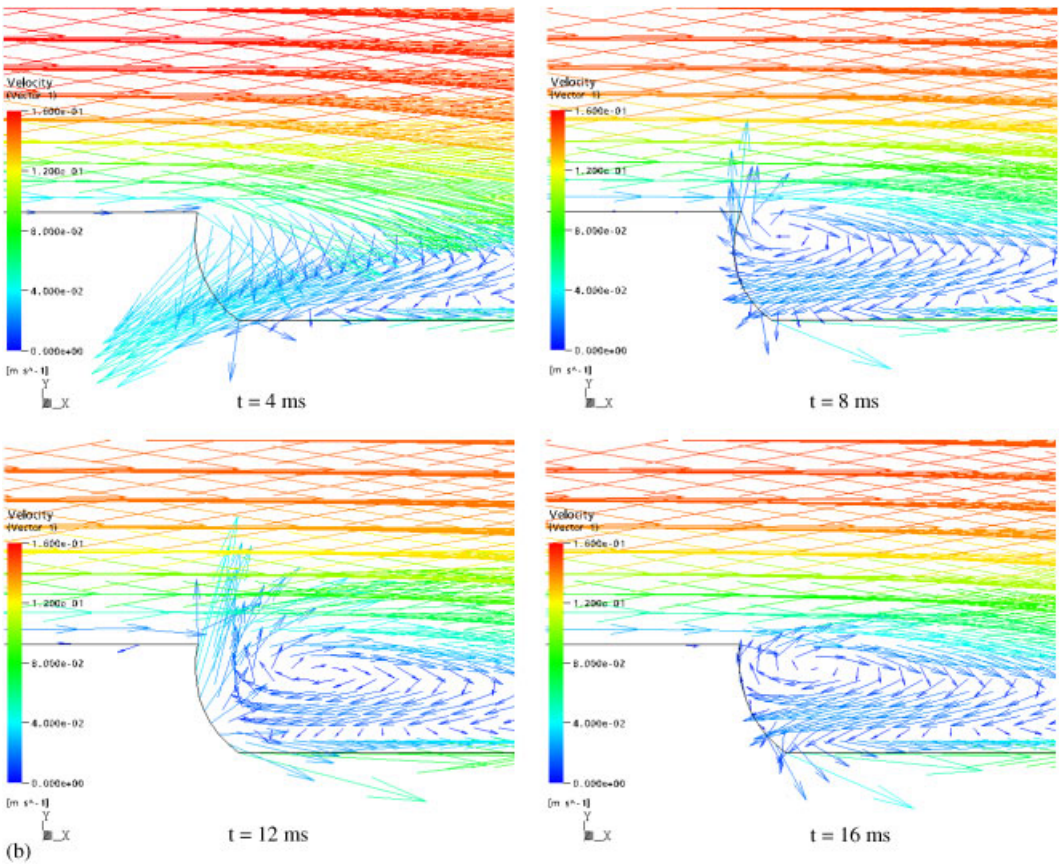

Figure 8. (Continued).

U_S does not appear to play a significant role on the natural frequency of the backward-facing compliant-step configuration, the flow patterns in the vicinity of the step are considerably affected as shown in Figure 8 for one period of compliant step motion. In Figure 8(a) the vector flow field is given with a stationary substrate, while in Figure 8(b) the solution is obtained with a substrate moving at 0.1 m/s. In both cases at $t = 4$ ms the contact line is receding into the step at a near peak speed, while at $t = 8$ ms the contact line approaches its final (receded) position and a velocity approaching zero. The line then moves forward with a peak speed close to $t = 12$ ms and a final forward stationary position at 16 ms. In both cases the recirculation zone appears to be nearly completely suppressed when the contact position is at its peak receding speed. The recirculation is also largest for the two cases when the line is at its peak forward velocity. The recirculation zone is reduced for situations where the substrate is in motion. The size of recirculation zone depends on the combination of flow rate, q, and substrate speed applied. In non-isothermal flow situations, particularly with strong cooling fluxes as occurring in metal processing, the modified recirculation pattern would likely influence the natural frequency of the compliant step due to temperature-dependent property variations.

DOI: 10.1002/fld

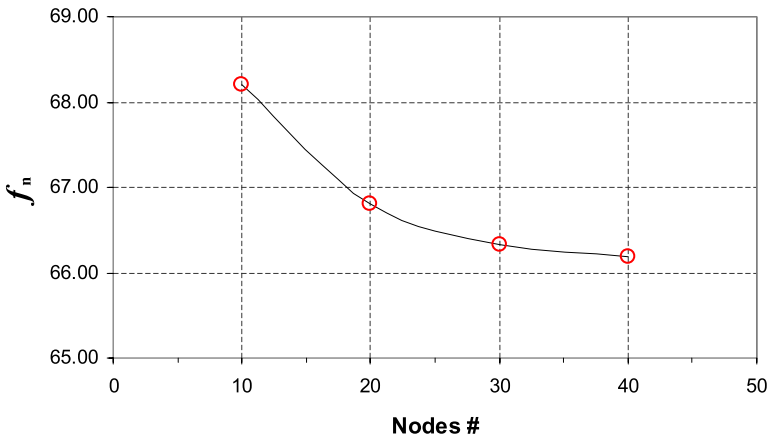

Figure 9. Effects of grid refinement on undamped natural frequency obtained with conditions as outlined in Table I (for aluminium).

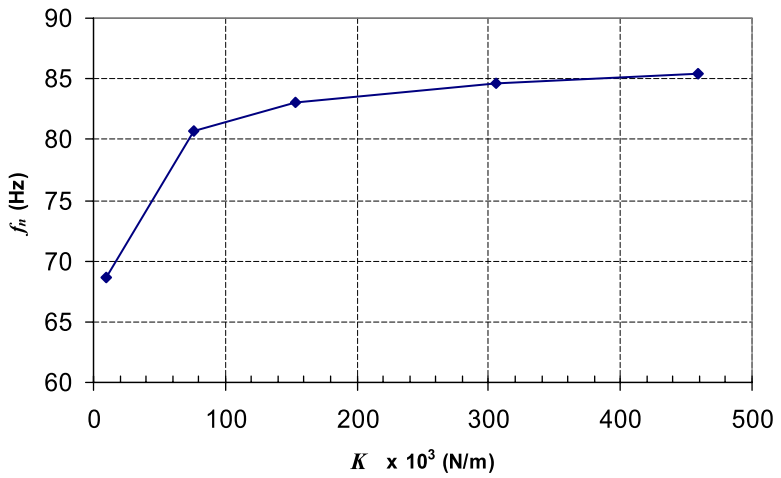

Figure 10. Natural frequency response for a compliant step membrane with different membrane constants. Results obtained with conditions as outlined in Table I for aluminium except for the use of Equation (7) for the interfacial tension model. Note that the total unstretched membrane length (Δs_0) is equal to $h/2$.

To test the sensitivity of these predictions to mesh density a grid refinement study was performed where the number of nodes defining the compliant step was increased from 10 to 40 in increments of 10. The effect of this grid refinement is shown in Figure 9 where a grid-independent solution occurs approximately at 40 nodes. The variation in predicted frequency over this range of node refinement is less than 3%.

Simulations were also conducted with the compliant step modelled as a membrane. Similar to the previous calculations, step input tests were conducted to obtain the natural frequency. Results obtained with aluminium as the working fluid and a range of membrane constants is shown in Figure 10 for a fixed head (conditions given in Table I). The results show an asymptotic limit of

DOI: 10.1002/fld

natural frequency at slightly over 85 Hz with increasing membrane constant K. This result does not follow closely the traditional $K^{1/2}$ behaviour of a spring–mass system since in our system the mass ($= \mathrm{d}\kappa/\mathrm{d}A \cdot 1/\rho$) depends also on the membrane constant. In particular, as the stiffness of the system increases (by increasing K) the curvature of the membrane decreases (increasing radius r) which leads to $(\mathrm{d}\kappa/\mathrm{d}A)_{\mathrm{eq}}$ becoming very small (by analogy see Figure A2 where the inverse of $\mathrm{d}\kappa/\mathrm{d}A$ is plotted for an interface based on a coefficient of surface tension). Viewing Equation (25) it is apparent that this would act to counter increases in the stiffness of the system modifying the asymptotic behaviour in natural frequency. In Equation (25) the stiffness is given by $\sigma h_1/L$ while for a membrane it would be $K\Delta s_0 h_1/L$ assuming membrane deflections are in the order of Δs_0 (an assumption reasonable for the results shown in Figure 10). The results in Figure 10 were obtained with the membrane free to move at the substrate at a fixed angle of 140° (similar definition as the contact angle). It is clear that with a membrane there may be other boundary models that could be developed, depending on the application, and that these could have a significant influence on the motion of the interface.

7. CONCLUSIONS

An approach has been developed for examining the compliant step response in a backward-facing boundary configuration, which represents closely the situation found in many continuous-casting processes where metal is delivered to a moving substrate. In these processes it is not clear what forces are active in the surface, i.e. surface tension forces or membrane-type forces, and therefore the present method has been developed to be flexible in examining both scenarios. The model developed here has been shown to reproduce the natural frequency behaviour for a simple dynamic system of flow in a channel with a flexible transition element using surface tension. The frequency response over a range of heads is well predicted, as well as the natural frequency response between water and aluminium scales in the expected manner. A grid sensitivity study indicates that the solution for these conditions approaches grid independence in the vicinity of 40 surface nodes. The model has also been shown to be extendable to the case of a membrane compliant step, where the substrate contact line must then be modelled with something other than a contact angle. The model chosen would be specific to the application being considered. The basis of the model is a finite-volume formulation of the fluid flow equations which are flexible for incorporating what will be the next investigation, and that is the influence of heat transfer on the compliant step response. Considering these more complex situations, for example with heat transfer present, and surface tension a strong function of temperature, the modified flow patterns may lead to changes in the natural frequency response. Furthermore, it will be possible to consider a combination of surface tension and membrane forces active at the surface, a situation applicable to metal oxides partially formed on the compliant step. This scenario is of interest in aluminium strip casting where oxides readily form over a free surface at elevated temperatures. The influence of a dynamic contact angle could also be investigated using some of the more recent models available in the literature.

APPENDIX A: MENISCUS GEOMETRY UNDER HYDROSTATIC CONDITIONS

The rate of change of the compliant step curvature to its area, defined as shown in Figure A1 with $A = A_1 + A_2$, can be obtained numerically on the basis of an analytical solution of the interface

DOI: 10.1002/fld

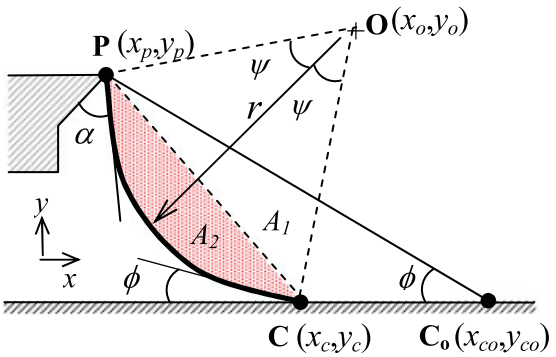

Figure A1. Nomenclature and area definition for a meniscus profile of fixed radius between point **P** and **C** used in verification of CFD solution.

position. Such a solution is possible under certain constraints such as fixed pressures before and behind the meniscus (implying a constant radius), and fixed contact angle as shown in Figure A1. On this basis an arc through the meniscus can be defined

$$(x - x_0)^2 + (y - y_0)^2 = r^2 \tag{A1}$$

with the slope at any location on this arc equal to

$$2(x - x_0) + 2(y - y_0)\frac{\mathrm{d}y}{\mathrm{d}x} = 0$$

or simply

$$\frac{\mathrm{d}y}{\mathrm{d}x} = -\frac{(x - x_0)}{(y - y_0)} \tag{A2}$$

At the substrate contact line the slope can be related to the tangent of the non-wetting contact angle, ϕ, such that

$$\left.\frac{\mathrm{d}y}{\mathrm{d}x}\right|_{\mathrm{c}} = -\frac{(x_{\mathrm{c}} - x_0)}{(y_{\mathrm{c}} - y_0)} = -\tan\phi \tag{A3}$$

Considering specifically the backward-facing compliant step geometry, the unknowns in determining the position of the interface are x_{c} and the arc centre x_0, y_0. Other positions x_p, y_p and y_{c} are known. This allows for three equations with three unknowns

$$1:\ (x_{\mathrm{c}} - x_0)^2 + (y_{\mathrm{c}} - y_0)^2 = r^2$$

$$2:\ (x_p - x_0)^2 + (y_p - y_0)^2 = r^2$$

$$3:\ \tan\phi = \frac{(x_{\mathrm{c}} - x_0)}{(y_{\mathrm{c}} - y_0)}$$

DOI: 10.1002/fld

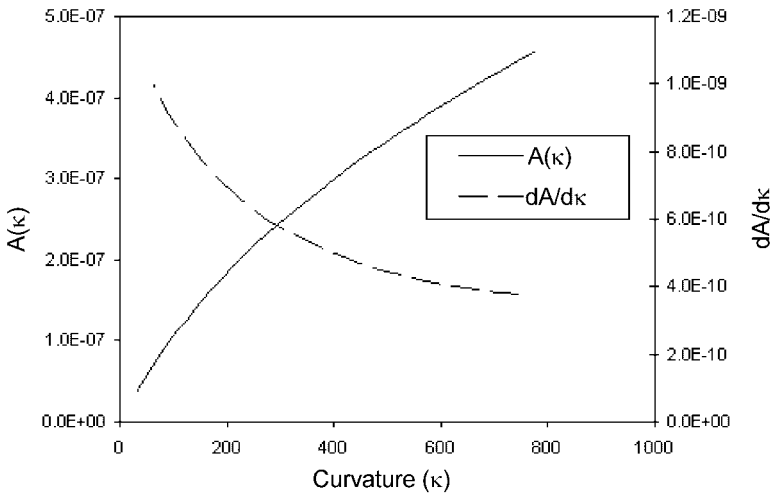

Figure A2. Meniscus area (A) *versus* curvature (κ) and associated derivative.

Assuming the interface to always be concave in shape, and the contact angle directed as shown in Figure A1, the solution with appropriate signs becomes

$$y_0 = y_p + \frac{r}{\sqrt{1 + (\tan\phi)^2}} \tag{A4}$$

$$x_0 = x_p + \left(\sqrt{r^2 - (y_p - y_0)^2}\right) \tag{A5}$$

$$x_c = x_0 - \frac{r}{\sqrt{1 + (\tan\phi)^{-2}}} \tag{A6}$$

The angle formed by the lines joining the centre of the arc and the contact lines is defined as 2ψ, in which

$$\sin\psi = \frac{\sqrt{(y_c - y_p)^2 + (x_c - x_p)^2}}{2 \cdot r} \tag{A7}$$

This enables the areas A_1 and A_2 to be computed as follows:

$$A_1 = \tfrac{1}{2}(y_p - y_{co})(x_{co} - x_c), \quad A_2 = r^2(\psi - \sin\psi \cdot \cos\psi) \tag{A8}$$

Choosing a pressure difference over the meniscus allows the radius to be computed (using Equation (17)), which then can be used with Equations (A4)–(A6) to obtain the arc centre and contact line location for the meniscus. This then allows the area of the meniscus region, A, to be calculated with Equations (A7) and (A8). A curve of $A(\kappa)$ can then be generated and numerically differentiated to obtain $\mathrm{d}A/\mathrm{d}\kappa$ needed in Equations (25) and (26). In Figure A2 the curve $A(\kappa)$ and its derivative are shown. The location for evaluating $(\mathrm{d}A/\mathrm{d}\kappa)_{eq}$ in Figure A2 is at κ_{eq} obtained from Equation (23).

It should be noted that there is a limit to the pressure that can be applied on the inside of the meniscus. When exceeded, the angle α indicated in Figure A1 will attain the contact angle ϕ on

DOI: 10.1002/fld

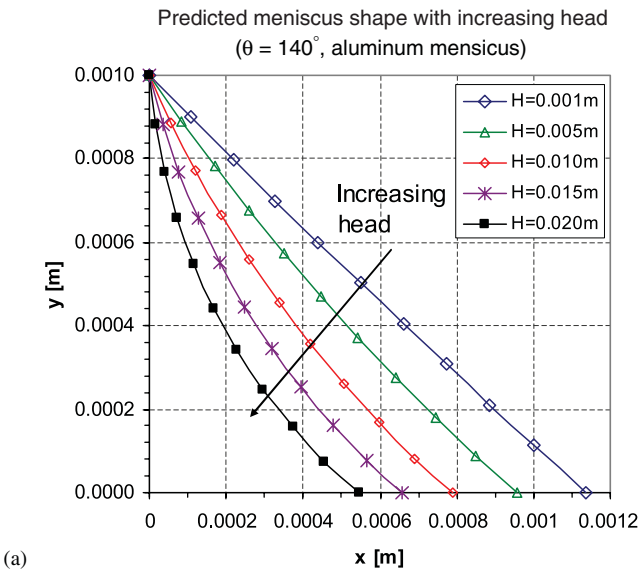

(a)

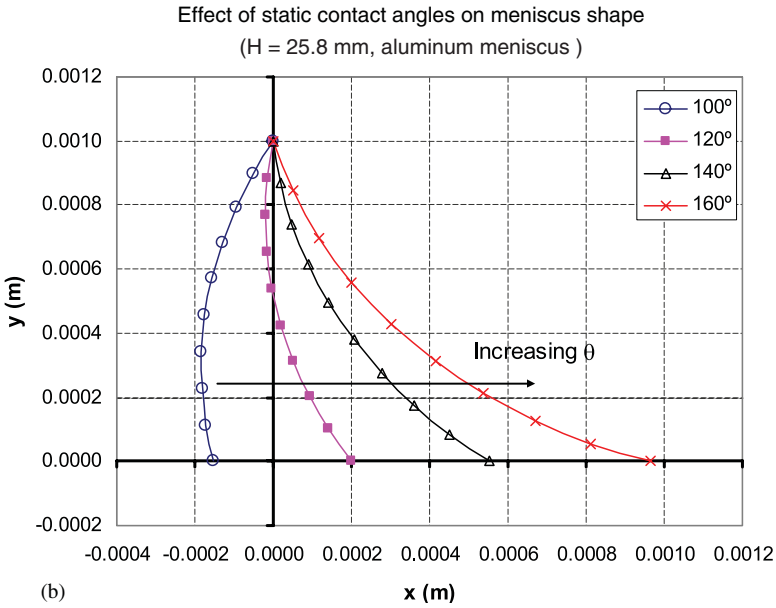

(b)

Figure A3. Compliant step static shape and contact line position as a function of: (a) head and (b) contact angle. Note that the inner contact angle θ is related to ϕ *via* the relation $\phi = 180 - \theta$.

the underside of the tip, a situation which forces the meniscus to recede underneath. This situation has not been considered, and is generally avoided by careful control of the pressure (although this control is complicated by the uncertainty of the contact angle under dynamic conditions). Figure A3 shows how the compliant interface, calculated based on the hydrostatic model above (Equations

DOI: 10.1002/fld

(A4)–(A6)) for computing the contact line location, will respond under different pressures and varying contact angles.

ACKNOWLEDGEMENTS

The authors would like to acknowledge the support of Novelis Inc. through an NSERC collaborative research and development grant (CRDPJ-248034).

REFERENCES

1. Gerber AG, Ng C, Gallerneault M. Surface-oriented melt/substrate eat-transfer model in aluminium strip casting. *Metallurgical Transactions B* 2004; **35B**:2004.
2. Gerber AG. Heat and mass transfer predictions of the early contact of a liquid metal on an intensely cooled moving substrate. *International Journal of Heat and Mass Transfer* 2005; **48**:2722–2734.
3. Barker SW, Gallerneault M, Sutter B. The effect of molten metal meniscus movement upon the surface microstructure. In *MetSoc*, *Proceedings of the Light Metals Symposium*, *Light Metals 2001*, Sahoo M, Lewis TJ (eds), Toronto, Ontario, August 2001; 133–146.
4. Raithby GD, Xu WX, Stubley GD. Prediction of incompressible moving-boundary flows with an element-based finite volume method. *Computational Fluid Dynamics Journal* 1995; **4**(3):353–371.
5. Xu W-X, Raithby GD, Stubley GD. Application of a novel algorithm for moving surface flows. *Journal of Hydrodynamics*, *Series B* 1997; **1**:87–95.
6. Dussan EB. On the spreading of liquids on solid surfaces: static and dynamic contact lines. *Annual Review of Fluid Mechanics* 1979; **11**:371–400.
7. Eggers J, Stone HA. Characteristic lengths at moving contact lines for a perfectly wetting fluid: the influence of speed on the dynamic contact angle. *Journal of Fluid Mechanics* 2004; **505**:309–321.
8. Eggers J. Toward a description of contact line motion at higher capillary numbers. *Physics of Fluids* 2004; **16**(9):3491–3494.
9. Walkley MA, Gaskell PH, Jimack PK, Kelmanson MA, Summers JL. Finite-element simulation of three-dimensional moving-boundary flow problems with dynamic contact lines. *International Journal for Numerical Methods in Fluids* 2004; **00**:1–6.
10. Schneider GE, Raw MJ. Control volume finite-element method for heat transfer and fluid flow using collocated variables—1. Computational procedure. *Numerical Heat Transfer* 1987; **11**:363–390.
11. Huh C, Scriven LE. Hydrodynamic model of steady movement of a solid/liquid/fluid contact line. *Journal of Colloid and Interface Science* 1971; **35**:85–101.
12. Eggers J. Existence of receding and advancing contact lines. *Physics of Fluids* 2005; **17**:082106.
13. Hutchinson BR, Galpin PF, Raithby GD. Application of additive correction multigrid to the coupled fluid flow equations. *Numerical Heat Transfer* 1988; **13**:133–147.
14. Raw MJ. A coupled algebraic multigrid method for the 3D Navier–Stokes equations. *Proceedings of the 10th GAMM Seminar*, Kiel, Germany, 14–16 January. Notes on Numerical Fluid Mechanics, vol. 49. Vieweg-Verlag: Braunschweig, Wiesbaden, Germany, 1995.
15. Macleod I. An isothermal water model of continuous aluminium sheet casting. *Masters of Science in Engineering Thesis*, University of New Brunswick, Fredericton, Canada, June 2006.

DOI: 10.1002/fld